Interaction and Deformation of Elastic Bodies: Origin of Adhesion Hysteresis

Phil Attard†

Ian Wark Research Institute, University of South Australia, Mawon Lakes, SA 5095, Australia

Received: May 23, 2000; In Final Form: August 29, 2000

The deformation and adhesion of soft elastic particles interacting with a Lennard-Jones potential is obtained by solving self-consistently the elasticity equations. Hysteresis is demonstrated between loading and unloading. Also, the pull-off force or maximum adhesion is shown to increase and eventually to saturate as the maximum applied load is increased. The origin of both of these phenomena, which have been observed experimentally, is traced to limited equilibration and dynamic hysteresis of the shape and contract angle between the advancing and receding deformed solids.

Introduction

The adhesion of particles to each other or to a substrate occurs in many areas of applied science and technology, and hence its measurement, understanding, and control is important. Adhesion is related to the surface energy of the solids, which is a fundamental quantity dependent upon the surface chemistry and the molecular structure of the solid, and the nature of the adjacent fluid interface. Also important is the elasticity of the particles, since all solids are deformable to varying degrees, and their change in shape when they interact is affected by their adhesion and by the applied load. This interdependence of adhesion and deformation complicates the quantitative analysis and interpretation of data and creates ambiguities in the value of the surface energies derived from measurements.

The adhesion may be defined as the negative of the pull-off force F, and one of the earliest results that relates this to the surface energy γ is due to Johnson, Kendall, and Roberts (JKR)[1]

$$F = -\frac{3}{2}\pi\gamma R \tag{1}$$

where R is the particle radius. Alternatively, Derjaguin, Muller, and Toporov (DMT)[2] obtained

$$F = -2\pi\gamma R \tag{2}$$

The discrepancy between these two, which has been the source of long-standing controversy,[1−4] stems in part from the approximate nature of the analysis. Both are based on contact mechanics, which assumes that their exists a strictly flat region of contact between the particles and that the particles experience an infinitely short-ranged interaction in this region and do not interact outside of it.

In an effort to resolve the above discrepancy, and to obtain quantitative relationships between the adhesion and the surface energies, a number of authors have calculated the elastic deformation of the solids using realistic surface forces of finite range.[5−14] Their general conclusion is that DMT theory is applicable for hard solids with small adhesions and that JKR theory becomes increasingly applicable at the soft solid, large adhesion end of the spectrum.

Attard and Parker[11] solved the elasticity equations numerically and obtained self-consistently the deformation of the solids as a function of the applied load using a realistic Lennard-Jones model of the van der Waals interaction. In modeling typical experiments, hysteresis was found between the loading and unloading branches, and for soft, adhesive solids, it was found that the pull-off force was not unique. These results contradicted the JKR and DMT equations and called into question the quantitative validity of extracting the surface energy from the measured pull-off force.

Two types of hysteresis were found by Attard and Parker.[11] First, the position at which the bodies jumped into contact was smaller than that at which they jumped apart. This phenomenon, which has also been found by simulations[9,10] is due in part to the finite range of the van der Waals interaction and obviously cannot be predicted by JKR or other contact theories. Second, it was found that the deformation-loading curve did not coincide with the deformation-unloading curve even when both corresponded to contact and that the maximum tension on unloading, which is the negative of the pull-off force, depended upon the value of the maximum applied load. This predicted hysteresis and nonunique pull-off force has serious repercussions for the measurement of adhesion and deformation of soft solids. For this reason, and because the hysteresis contradicts the long-standing ideas embodied in JKR and DMT theory, confirmation of these results is desirable. There is in fact a deal of experimental evidence to show that the pull-off force is highly variable and that it does not have a unique value (e.g., see refs 15−17). For soft bodies with large adhesions, experimental measurements show that the pull-off force is hysteretic, depending upon the history of the sample, and the details of the loading-unloading cycle.[17−28] Taken together these experimental measurements confirm the predictions of Attard and Parker,[11] at least qualitatively. In addition, the method of Attard and Parker[11] has been used to quantitatively describe experimental data.[29,30] In view of this experimental evidence and of the relatively sophisticated calculations, there is some doubt about the quantitative applicability of the DMT and JKR approximations to actual measured data. It is difficult to check the validity of the DMT and JKR approximations experimentally because of the lack of an independent method for measuring the surface energy.

† E-mail: phil.attardi unisa.edu.au.

10.1021/jp0018955 CCC: $19.00
Published on Web 10/21/2000

This paper aims to explore in detail the adhesion hysteresis with a view to elucidate the physical origin of the measured phenomena[15−28] and to propose quantitative experimental tests. The present calculations improve upon earlier work on elastic deformation due to finite ranged surface forces[5−14] by using more refined numerical parameters and computational algorithms. A unique feature of the present approach is that it duplicates the actual experimental procedures. The present work confirms the existence of the hysteresis identified by Attard and Parker,[11] and it goes beyond that work by focusing in detail upon the hysteresis, which has allowed it to be studied for a variety of cases and its underlying cause to be identified.

I. Theory

A. Model and Analysis. Consider two interacting spheres with radii R_1 and R_2. For undeformed spheres, $h_0(r)$ denotes the local surface separation measured at a lateral distance r from the central axis (the line connecting the centers of the spheres). The distance of closest approach of the undeformed surfaces is denoted by $h_0 \equiv h_0(0)$, and for separations much less than the radii simple geometry gives

$$h_0(r) = h_0 + \frac{r^2}{2R} \tag{3}$$

Here

$$R^{-1} \equiv R_1^{-1} + R_2^{-1} \tag{4}$$

is the effective radius; for two identical spheres, R is half their radius, and for a sphere interacting with a planar substrate it is the sphere's radius. More generally, R may be given in terms of the principal radii of curvature of the bodies.[31]

Because of their mutual interaction the spheres deform. Let the actual local surface separation be given by

$$h(r) = h_0(r) - u(r) \tag{5}$$

where the total deformation is

$$u(r) = u_1(r) + u_2(r) \tag{6}$$

A negative deformation corresponds to flattening under load, and a positive deformation corresponds to bulging under tension. In the elastic half-space approximation, a normal point force induces a deformation of the surface that decays as r^{-1} away from the point of contact. Accordingly, if $p_\alpha(r)$ is the local pressure acting on surface α, then the deformation of that surface is[32]

$$u_\alpha(\mathbf{r}) = -\frac{1-\upsilon_\alpha^2}{\pi E_\alpha}\int \frac{p_\alpha(\mathbf{t})}{|\mathbf{r}-\mathbf{t}|}\mathrm{d}\mathbf{t} \tag{7}$$

where for each solid labeled α, E_α is Young's modulus and υ_α is Poisson's ratio. For the present cylindrical symmetry one has

$$u_\alpha(r) = -\frac{1-\upsilon_\alpha^2}{E_\alpha}\int_0^\infty p\alpha(t)\, k(r,t) t\, \mathrm{d}t \tag{8}$$

where the kernel is

$$k(r,t) = \begin{cases} \frac{4}{\pi r}K(t^2/r^2) & t < r \\ \frac{4}{\pi t}K(r^2/t^2) & t > r \end{cases} \tag{9}$$

$K(m)$ being the complete elliptic integral of the first kind of parameter m.

The pressure $p_1(r)$ arises from the interaction with sphere 2, and vice versa. This local pressure depends on the local separation, and since it arises from the derivative of the interaction potential one has

$$p_1(r) = p_2(r) = p_s(h(r)) \tag{10}$$

where $p_s(h)$ is the pressure between two infinite parallel planes separated by h. This result is valid when $h_0 \ll R$, since surface forces are in general rapidly decaying and have a practical range much less than the effective radius. In view of this result the total deformation may be written

$$u(r) = \frac{-2}{E}\int_0^\infty p_s(h(t))\, k(r,t) t\, \mathrm{d}t \tag{11}$$

where the elasticity parameter is given by

$$\frac{2}{E} = \frac{1-\upsilon_1^2}{E_1} + \frac{1-\upsilon_2^2}{E_2} \tag{12}$$

For a given force law $p_s(h)$, at each undeformed separation h_0, eqs 5 and 11 must be solved self-consistently.

The total load is simply the integral of the surface force,

$$F = 2\pi\int_0^\infty p_s(h(r)) r\, \mathrm{d}r \tag{13}$$

The central deformation, which represents the flattening of the bodies, is defined as

$$\delta = h(0) - h_0 = -u(0) \tag{14}$$

In general, as the bodies are driven toward each other, the central deformation and the load become more positive. This is called loading. Conversely, unloading corresponds to a decreasing (more negative) central deformation and load as the centers of the bodies are separated. To distinguish between the deformed and undeformed separations, h_0 will be called the position, and h will be called the separation.

In this work a Lennard-Jones representation of the van der Waals attraction is used,

$$p_s(h) = \frac{A}{6\pi h^3}\left[\frac{z_0^6}{h^6} - 1\right] \tag{15}$$

Here A is the Hamaker constant and z_0, which characterizes the range of the short-range repulsion, is the equilibrium separation of planes under zero load. This Lennard-Jones law is the simplest realistic potential that embodies the long-range attraction and the short-range repulsion that occur in all real systems. In liquid systems there can be additional effects such as oscillatory forces at short-range due to solvent structure. These are not included here but have been studied previously in the context of elastic deformation[12] and of a quantitative analysis of experimental data that used both hard-sphere and Lennard-Jones models.[33]

The value of the surface energy, which is used in making comparison with JKR and DMT theory, is

$$\gamma = \frac{A}{16\pi z_0^2} \tag{16}$$

It turns out that the elasticity and adhesion may be combined

into the dimensionless parameter[11]

$$\sigma = \frac{\gamma\sqrt{R/z_0{}^3}}{E} \tag{17}$$

Large values of σ correspond to soft, adhesive particles. With this parameter, and using z_0 as a length scale, one may map the deformation results obtained for any system onto any other system with the same values of the parameters.

B. Computational Details. The numerical algorithm used to solve the equations mimicked a typical loading-unloading experiment, except that the displacement was controlled rather than the load. The three functions $u(r)$, $h(r)$, and $p(r) = p_s(h(r))$ were defined on a grid, $0 < r < R^{max} \ll R$. In most of the results reported here $R = 10\ \mu$m, and the grid was of uniform spacing, $r_n = n\Delta - \Delta/2$, $n = 1, 2, ..., N$, with $\Delta = 1.5$ nm, $N = 1000$, and $R^{max} = 1.5\ \mu$m. Tests were made with up to 2000 nodes, and it was found that the results were not very sensitive to the choice of grid or spacing. The number of nodes used here is about an order of magnitude greater than that used previously in simpler studies.[13]

Upon discretization, the kernel, eq 9, became a matrix with elements $k_{nj} = k(r_n, r_j)$, and this was constructed using the fast nome expansion of the elliptic integrals, (cf. eqs 3.11 and A4 of ref 34). The deformation, eq 11, became

$$u_n = \frac{-2\Delta}{E}\sum_{j=1}^{N} k_{nj} r_j p_j \tag{18}$$

This assumed that the surface separation at R^{max} was large enough so that $p_N = p_s(h_N)$ was negligible. The logarithmic singularity at $r = t$, $K(m) \sim \ln[4\sqrt{1-m}]$ as $m \to 1$, was handled by integrating it analytically over the grid width, so that

$$k_{nn} = \frac{1}{r_n\Delta}\int_{r_n-\Delta/2}^{r_n+\Delta/2} \mathrm{d}t\, t k(r_n,t)$$

$$= \frac{1}{r_n\Delta}(I_{n+} + I_{n-}) \tag{19}$$

with

$$I_{n-} = \left(\frac{\Delta}{\pi} - \frac{\Delta^2}{4\pi r_n}\right)\left[1 + \ln\frac{16 r_n{}^2}{r_n\Delta - \Delta^2/4}\right] \tag{20}$$

and

$$I_{n+} = \frac{\Delta}{\pi}\ln\frac{16(r_n + \Delta/2)^2}{r_n\Delta + \Delta^2/4} + \frac{4r_n}{\pi}\ln\frac{2r_n + \Delta}{2r_n + \Delta/2} \tag{21}$$

It is evident that as $\Delta \to 0$, the contribution to the deformation from this logarithmic singularity is negligible.

On the loading branch the solids are driven toward each other at a uniform rate beginning at a large separation h_0 such that $p_s(h_0) \approx 0$, and the surfaces are undeformed ($u(r) = 0$, $h(r) = h_0(r)$). A cycle of convergence iterations began with a change in h_0 to $h_0 - d$, *at constant surface separation.* This means that the deformation was changed to $u(r) - d$, and $h(r)$ and $p(r)$ were unchanged. The step was $d = 0.05$ nm, which is between two and three times finer than that used in previous work.[11,13] The iterations in the cycle consisted of calculating in turn a new deformation profile, eq 11, separation profile, eq 5, and pressure profile, eq 10. The new deformation was mixed with the old deformation to ensure convergence. The mixing ratio was automatically decreased if oscillations or growth in the change in the central displacement was detected and otherwise was allowed to increase up to a value of 0.2. The iterations were terminated when the root-mean-square change in deformation, $\epsilon = [\sum_n u_n{}^{new} - u_n{}^{old})^2]^{1/2}/N$, was small enough. The case $\epsilon = 1$ pm typically took 500−1000 iterations per step in position. A typical loading−unloading curve took on the order of 500 steps, and it required on the order of a trillion floating point operations. Decreasing the convergence parameter to 0.1 pm increased the number of iterations by about an order of magnitude. After convergence the total load was calculated, and if required, the surface profiles were stored, before taking another step in position and recommencing the convergence cycle. For loading, $d > 0$. The unloading ($d < 0$) commenced with the deformation from the end of the loading path. This point, which corresponds to the maximum applied load, is here called the turning point.

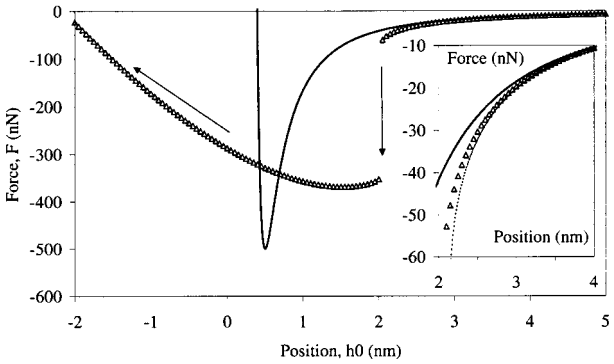

Figure 1. Force between two particles of effective radius $R = 10\ \mu$m. The Hamaker constant is 10^{-19} J, and the equilibrium separation is $z_0 = 0.5$ nm, giving a surface energy of $\gamma = 7.96$ mN m^{-1}. The bold curve is the rigid case, and the symbols are for an elasticity of $E = 10^9$ N m^{-2}, which gives $\sigma = 2.25$. For the latter, the force is calculated upon approach, and negative positions would correspond to interpenetration of the surfaces if deformation had not occurred. The inset compares the calculated force (symbols) with that for rigid spheres (bold), and the analytic approximation (dotted) discussed in the text.

It is emphasized that the above numerical procedure duplicates the experimental protocol. Generally an experiment consists of driving the surfaces toward each other at fixed velocity until the maximum load, at which point the motion is reversed. The equilibration time for the deformation and expansion of the contact area is controlled by the drive velocity. Similarly, in the computations the motion of the spheres is monotonic on each branch, and the equilibration time is controlled by varying the convergence parameter. Limiting the number of iterations in this way limits the distance that the contact line can move before the separation is changed. Reducing the speed of the solids is equivalent to increasing the number of iterations per step. Immediately following a step in position, the initial movement of the contact line is quite fast (large thermodynamic force). The motion slows as it approaches the equilibrium deformation.

In these computations full equilibrium is never attained before the surfaces move on. The motion appears to be overdamped, reaching a quasi-steady state that depends on the velocity of the solids.

Results

The force between two colloidal spheres is shown in Figure 1. The effective radius is $R = 10\ \mu$m and the effective elasticity is $E = 10^9$ N m^{-2}, which correspond to relatively soft solids

with strong adhesions, $\sigma = 2.25$. For the rigid, undeformed spheres (bold curve), the Lennard-Jones interaction is plotted. Using eqs 3 and 15 this is

$$F(h_0) = 2\pi\int_0^\infty \mathrm{d}r\, r p_s(h_0(r)) = \frac{AR}{6h_0^2}\left[\frac{z_0^6}{4h_0^6} - 1\right] \tag{22}$$

The right-hand side may be recognized as $2\pi R$ times the interaction free energy per unit area between planar bodies separated by h_0, as given by the Derjaguin approximation.[31] The attraction at long range and the steep but soft repulsion at short range are the two features in the curve that make it a realistic representation of the van der Waals interaction present in real systems. It is these that distinguish the present approach from the zero range potentials invoked in contact mechanics.

Three distinct consequences of elastic deformation may be seen in Figure 1. First, at larger separations the attraction has a higher magnitude for deformable particles than for rigid ones. This is mainly due to the fact that the particles bulge out toward each other, so that their actual surface separation is smaller than the nominal separation h_0 of the rigid particles (see below). Second, at a finite separation the surfaces jump into contact due to an elastic instability; the rate of energy decrease due to the steep gradient of the van der Waals attraction exceeds the rate of energy increase of elastic deformation. Third, as the particles are driven toward each other the force increases and turns from attractive to repulsive much more gradually than for rigid particles. Although the actual separation h always remains positive, the nominal separation or position h_0 becomes negative as the particles flatten. This soft contact region contrasts with the very steep repulsion evident for rigid particles.

The inset to Figure 1 shows the force at large separations prior to the jump into contact. Both curves are the van der Waals force given above, with the bold curve, $F(h_0)$, using the nominal separation, h_0, and the dotted curve, $F(h)$, using an approximation to the actual separation, $h = h_0 + \delta$. The central deformation used here is negative due to the particles bulging toward each other under the influence of the attraction, and consequently, the actual van der Waals attraction is larger than the nominal one, $|F(h)| > |F(h_0)|$. The amount of this precontact bulge is given to a very good approximation by[11]

$$\delta = \frac{-A\sqrt{2R}}{8Eh^{5/2}} \tag{23}$$

where $h \equiv h(0)$. This equation is best used to give h_0 as a function of h. The inset to Figure 1 shows that using this approximation, $F(h)$ is more accurate than $F(h_0)$ for the precontact force. Whereas $F(h_0)$ underestimates the attraction, close to the jump into contact $F(h)$ begins to overestimate the actual interaction of the deformable spheres. However, it is evident from the inset that the primary effect of deformation on the force between particles prior to contact is due to the change in the actual surface separation as they bulge toward each other.

Figure 2 compares the amount of precontact bulge given by the above analytic approximation with that obtained by the full numerical calculations. It may be seen that the approximation is quantitatively accurate over most of the regime shown. Just prior to the jump into contact, the deformation begins to be overestimated by the above approximation. This is the main reason for the overestimation of the force by the approximation in the inset of Figure 1.

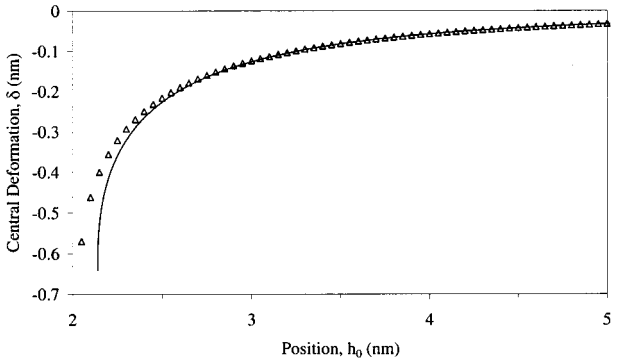

Figure 2. Bulge prior to contact for the deformable sphere of the preceding figure. The symbols are the numeric calculations and the curve is the approximation eq 23.

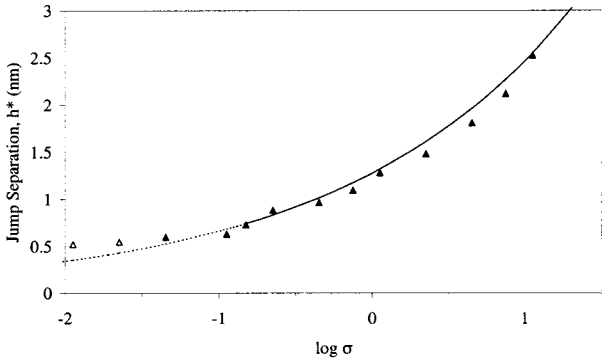

Figure 3. Actual separation at which the surface jumps into contact due to elastic instability as a function of the elasticity parameter σ ($z_0 = 0.5$ nm). The symbols are the numeric results (the open symbols signify the last separation prior to contact in the case of more rigid spheres when no jump can reliably be identified). The curve is the analytic approximation, eq 24 (shown dotted when the instability criterion cannot actually be satisfied). The resolution of the numeric results is 0.05 nm, and the logarithm is base 10.

As mentioned above, at a separation when the gradient of the attraction exceeds the rate of increase of elastic energy, the surfaces jump into contact. This jump is an inherent property of the solids, and occurs no matter how rigidly the position of the particles is controlled. The critical jump separation is plotted in Figure 3 against the adhesion−elasticity parameter σ. Small values of a represent small, hard particles with low adhesions, and large values of σ correspond to large, soft, adhesive particles. Also shown is an analytic approximation to this critical separation,[11]

$$h^* = \left(\frac{3A\sqrt{2R}}{8E}\right)^{2/7} \tag{24}$$

It can be seen that this analytic approximation is very good and that it correctly predicts the limit of stability of noncontact interactions over some 3 orders of magnitude of the adhesion−elasticity parameter.

Figure 4A shows the shape of the particles as they deform during loading. Close inspection of the profiles prior to contact shows the bulge discussed above, and the sudden jump into contact. Once in contact the surfaces appear flat, so that on the scale of the figure there is no ambiguity about where the surfaces are in contact. In contact the surface separation is $h(r) \approx z_0$, it being less than the equilibrium separation toward the center and greater than it toward the contact periphery. This finite curvature

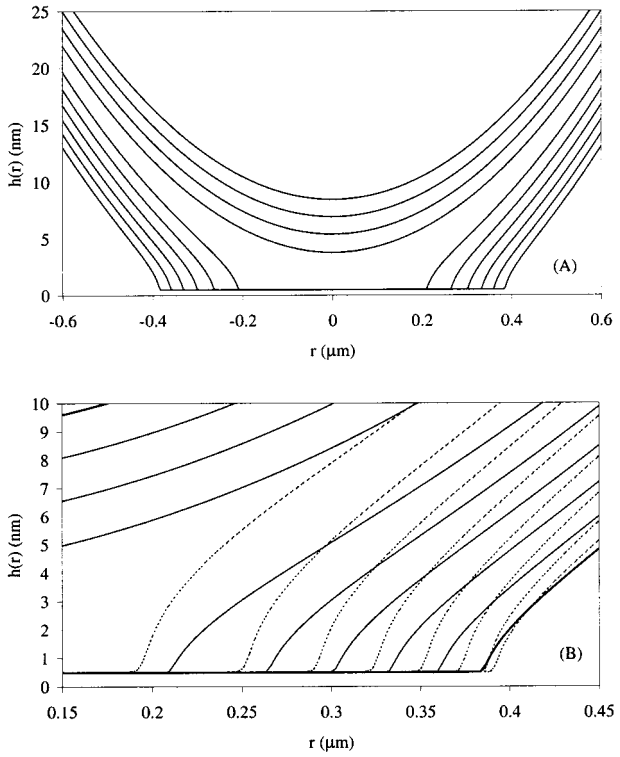

Figure 4. (A) Shape of the elastic particles upon approach, plotted as a sphere interacting with a flat. (All parameters are as in Figure 1 except that $E = 3 \times 10^8$ N m^{-2}, which gives $\sigma = 7.50$.) The abcissa is the lateral distance from the axis of cylindrical symmetry, and the ordinate is the local separation. The curves are snapshots at positions of, from bottom to top, $h_0 = -5$, -3.5, -2, -0.5, 1, 2.5, 4, 5.5, 7, and 8.5 nm. Note that due to the different scales used on the two axes, the undeformed sphere (top) appears as a parabola. (B) Detail of the shape on approach (solid curves) and on retraction (dashed curves) at the same positions as in (A). The loading and unloading curves are coincident (bold solid curves) at the turnaround point, $h_0 = -5$ nm, and at the furthest separation, which us just after the jump from contact, $h_0 = 8.5$ nm. Note that contact area upon unloading is greater than the corresponding loading case and that the contact area at $h_0 = -3.5$ nm (unloading) is actually greater than at $h_0 = -5$ nm.

of the contact region is due to the finite range of the van der Waals attraction and is a general feature of soft contact problems. The ambiguity it creates in defining the contact area does not have serious practical ramifications (see below).

Following the initial jump into contact the contact area grows rapidly to a finite value. As the solids are pushed together the contact line expands at a steady rate. In the case of Figure 4A, the contact radius has reached 0.38 μm at the turning point. If the solid bodies are being driven together at 1 μm/s, the velocity of the contact line, which was greater than 100 μm/s initially following the jump into contact, has reached a steady 20 μm/s at the turning point.

Figure 4B compares in detail the surface profiles on the loading and the unloading branches. At any given position h_0, the contact area is greater on the unloading branch than on the loading branch. Indeed, after the direction of motion of the solids has been reversed, the contact area continues to expand for a short time. The surfaces remain in contact on the unloading branch *after* the separation h_0* at which they jumped into contact on approach. The speed of the contact lines increases as the pull-off point is approached, reaching 150 μm/s for a driving speed of 1 μm/s.

It can be seen in Figure 4B that during unloading the sphere is more "stretched" than during loading. The exterior angle

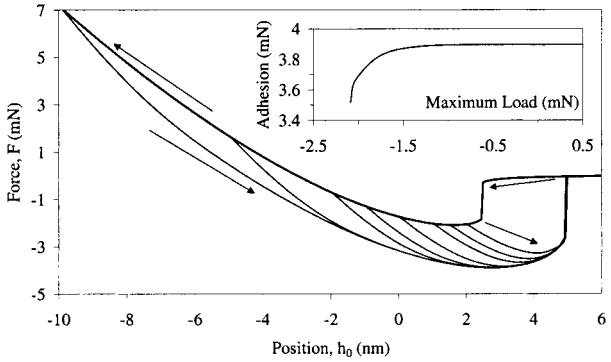

Figure 5. Force as a function of nominal separation ($R = 1.5$ cm, $E = 10^{11}$ N m^{-2}, $A = 5 \times 10^{-19}$ J, and $z_0 = 0.5$ nm, which give $\sigma = 4.36$ and $\gamma = 39.8$ mN m^{-1}). The loading curve is shown bold, and the unloading curves commence at nominal separations of, from left to right, $h_0 = -10$, -5, -2, -1, 0, 1, 1.5, and 2 nm. Inset: Adhesion (maximum tension) as a function of the maximum applied load (the force at the turn).

between the tangent of the deformed sphere (measured in the apparently linear asymptotic region) and the planar substrate is $\theta_{1v2} = 49.7$ mrad on approach and 53.7 mrad on separation. That is, the receding contact angle is greater than the advancing one.

Figure 5 shows the force for deformable particles as a function of drive position during both the loading and unloading. It can be seen that the two branches are quite distinct and that there is obvious hysteresis in the figure. In these circumstances the unloading branch depends on the turning point, which is the maximum load applied before reversing direction. After reversal, one can identify a transitory regime for each of the individual unloading curves before they coalesce onto a single trajectory, which in essence is the envelope of the transitions. In general each individual trajectory has a minimum, which is its pull-off force. After this the trajectory is unstable for controlled load but remains stable for the present calculations, which mimic a controlled displacement experiment. Finally, a point of instability is reached at which the surfaces jump apart. The load at this point represents the controlled displacement pull-off force and is the same for all trajectories.

The enveloping curve has a minimum, which represents the pull-off force of the trajectories that pass through it. If the maximum applied load is large enough (i.e., large enough penetration or turning point), the transition period ends prior to this minimum and the actual pull-off force for the individual trajectory corresponds to the one on the envelope. However, for a trajectory with a small maximum applied load, the minimum force is greater than that on the envelope, and consequently, the measured adhesion will be decreased. This is shown in the inset of Figure 5 where the adhesion, which is the negative of the minimum unloading force, is plotted against the maximum applied load. It can be seen that for small applied loads the adhesion increases with load. As the maximum applied load is increased (deeper penetration or greater displacement before reversing direction), the adhesion continues to increase until it eventually saturates.

Qualitatively similar behavior is exhibited in Figure 6. Although the adhesion−elasticity parameter is larger in this system ($\sigma = 17.43$, compared to $\sigma = 4.36$ in Figure 5), the actual force is about an order of magnitude smaller for comparable displacements. This because the surface energy is smaller here, $\gamma = 7.96$ mN m^{-1}, than the $\gamma = 39.8$ mN m^{-1} of Figure 5. This is consistent with the JKR and DMT expressions, which predict that the adhesion is proportional to the surface

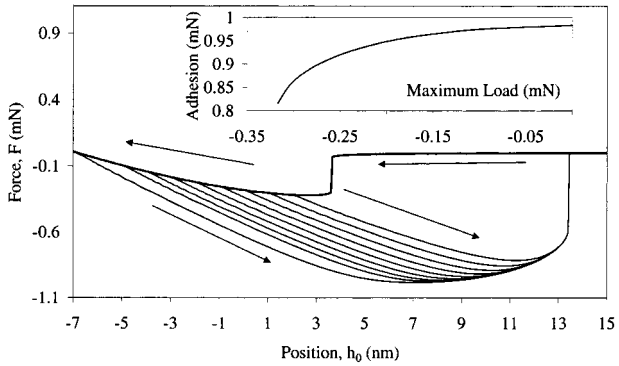

Figure 6. Same as the preceding figure but with $E = 5 \times 10^9$ N m^{-2} and $A = 1 \times 10^{-19}$ J, which give $\sigma = 17.43$ and $\gamma = 7.96$ mN m^{-1}. The unloading curves commence at nominal separations of, from left to right, $h_0 = -7$, -5, -4, -3, -2, -1, 0, 1, and 2 nm.

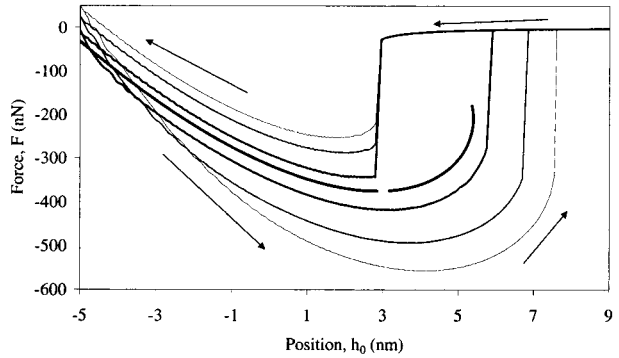

Figure 7. Force as a function of position for the parameters of Figure 4. The pairs of curves are for an accuracy of $\epsilon = 1$, 0.5, and 0.1 pm, from outside to inside (light to heavy), respectively. The unpaired bold curve is the JKR equilibrium prediction, with the break signifying the commencement of controlled displacement.

energy and independent of the elasticity. The dimensionless force,[11] $\bar{F}(\sigma) = F/E\sqrt{Rz_0^3}$, is about 6 times larger for the system of Figure 6 than for that of Figure 5 due to the larger adhesion−elasticity parameter.

Figure 7 shows the force-displacement hysteresis for various values of the convergence parameter ϵ. Smaller values of ϵ correspond to longer equilibration times and slower driving velocities. It can be seen that the hysteresis increases with increasing velocity. Conversely, the discrepancy between the loading and unloading branches decreases as the equilibration time is increased. It appears that they will eventually coalesce about the JKR prediction, so that it may be concluded that JKR represents an approximation to the static solution. It was not possible to perform the present calculations statically (i.e., with an infinite equilibration time, or with a convergence parameter of zero). This is of course also the experimental situation, since in practice the measurements are always performed dynamically.

The speed with which the contact line moves is plotted in Figure 8 for the case when the particles are driven together with velocity $\dot{h}_0 = \pm 1$ μm/s. For soft contact problems with their finite ranged interactions, the definition of contact is problematic. From Figure 4, a reasonable and practical protocol can be based on the minimum in the Lennard-Jones potential, which occurs at $z_0 = 0.5$ nm. Here the surfaces were defined to be in contact whenever the separation was less than $1.1z_0$. The sharpness of the transition between contact and noncontact evident in Figure 4 means that very similar results would be obtained using any other reasonable definition of contact. In Figure 8 it can be seen that the initial high rate of expansion of the contact area

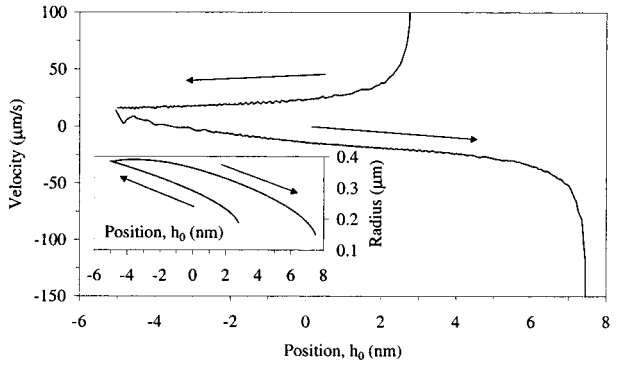

Figure 8. Velocity of the contact radius as a function of the position for a driving velocity $\dot{h}_0 = 1$ μm/s ($R = 10$ μm, $A = 10^{-19}$ J, $z_0 = 0.5$ nm, and $E = 3 \times 10^8$ N m^{-2}, which give $\gamma = 7.96$ mN m^{-1} and $\sigma = 7.50$). The surfaces were defined to be in contact whenever the local separation was less than $1.1z_0$. Inset: Contact radius itself as a function of the displacement during loading and unloading.

following the jump into contact slows to a relatively steady value ($\approx$20 μm/s) as the load is increased. Immediately following the turnaround, the velocity briefly remains positive (continued expansion) before the contact area shrinks at an increasing rate. At the point of maximum tension, the velocity of the contact line is approximately -25 μm/s, and by the minimum contact area it is moving at over -100 μm/s. The inset to Figure 8 shows the actual contact radius as a function of the drive position. It can be seen that at a given displacement, the contact radius during unloading is greater than during loading. This is a consequence of the lag in the deformation due to the finite drive velocity and the limited equilibration time.

Conclusion

This paper has been concerned with the effect of elastic deformation on the interaction and the adhesion of particles. Using the equations of linear elasticity, the deformation due to a spatially varying pressure profile was obtained. The pressure arises from the proximity of the surfaces of the two particles, and it depends on the local separation, which in turn depends on the deformation. A relatively realistic Lennard-Jones form for the surface force was used, and the numerical algorithm that was used duplicated a typical force measurement experiment.

It was found that deformation occurred prior to contact as the surfaces bulged toward each other under the influence of the attractive van der Waals part of the Lennard-Jones potential and that the interaction force between the particles was consequently larger than that for rigid particles. At a critical separation the particles jumped into contact due to an elastic instability, as has previously been predicted.[9−11] Analytic approximations for the precontact deformation and the critical separation due to Attard and Parker[11] were shown to be quite accurate. In contact, a relatively flat region was observed that increased with increasing applied load or displacement.

For soft bodies with large adhesions, hysteresis was observed between the loading and unloading branches of the measured force versus deformation curves, in agreement with previous work.[11] (The interaction pressure itself is nonhysteretic.) Here it was shown that the hysteresis in the force had its origin in the hysteresis in the deformation of the particles. Specifically, the receding contact angle was found to be greater than the approaching one. Also the contact area on loading was less than that at the same displacement upon unloading. Because of a transitory regime following the turning point, the pull-off force

increased with increasing maximum applied load until it saturated at large enough loads to allow a steady state to be established.

The hysteresis in the system was shown to depend on the amount of time the system was give to equilibrate, which in turns depends on the speed of approach or of separation of the particles. The hysteresis decreased with decreasing velocity. It appears that the JKR and DMT represent approximations to the equilibrium situation, which might be attained in an idealized static measurement. In practice adhesion is always measured dynamically, and so the present results represent a quantitative approach to analyzing experimental data. Accordingly, the hysteresis found here should be considered a viscoelastic phenomenon, with the dissipation due to the damping introduced into the computational algorithm.

Several experimentally testable predictions have emerged from the present calculations. First, the interaction of adhesive particles in contact is hysteretic between loading and unloading. The load is less (i.e., more negative) on the unloading branch at a given displacement, and the contact radius is greater on the unloading branch at a given load or a given displacement. Second, the hysteresis increases with the surface energy and the deformability of the particles. Third, the hysteresis increases with the speed of the measurement. Fourth, the adhesion (the negative of the pull-off force, or the maximum tension) increases with maximum applied load for small loads and saturates for large loads. Fifth, the adhesion decreases with decreasing speed of measurement and reaches an asymptote for slow enough velocities. For soft enough particles the value of this asymptote is given by the JKR static approximation. Sixth, since any pause between loading and unloading increases the initial unloading contact area, at a given measurement speed the adhesion increases with increasing dwell time and saturates for large dwell times.

There are a number of experimental measurements that show variability and hysteresis in the interaction and the adhesion of soft elastic particles.[15−28] Each of these papers presents data that support one or more of the specific predictions listed in the preceding paragraph. Hysteresis is of course a nonequilibrium phenomenon, and its magnitude is time and velocity dependent. Hence these experiments, and the present calculations, may be considered viscoelastic, which phenomenon has been explored in detail in the fields of peeling and crack propagation.[35,36] One may argue that in the limit of low elasticity all solids become viscoelastic, and hence the JKR equilibrium result may never be quantitatively applicable and that in all cases one should account for the dynamics of the measurement, as has been done here. The present theory can be said to be in accord with experiment, at least qualitatively. Quantitative experimental verification is foreshadowed.

Acknowledgment. The support of the Australian Research Council through the Special Research Centre for Particle and Material Interfaces at the Ian Wark Research Institute is gratefully acknowledged.

References and Notes

(1) Johnson, K. L.; Kendall, K.; Roberts, A. D. *Proc. R. Soc. London A* **1971**, *324*, 301.
(2) Derjaguin, B. V.; Muller, V. M.; Toporov, Yu. *J. Colloid. Interface Sci.* **1975**, *53*, 314.
(3) Tabor, D. *J. Colloid Interface Sci.* **1977**, *58*, 2.
(4) Maugis, D. *J. Colloid Interface Sci.* **1992**, *150*, 2243.
(5) Muller, V. M.; Yushchenko, V. S.; Derjaguin, B. V. *J. Colloid Interface Sci.* **1980**, *77*, 91.
(6) Muller, V. M.; Yushchenko, V. S.; Derjaguin, B. V. *J. Colloid Interface Sci.* 1983, *92*, 92.
(7) Hughes, B. D.; White, L. R. *Q. J. Mech. Appl. Math.* **1979**, *32*, 445.
(8) Hughes, B. D.; White, L. R. *J. Chem. Soc., Faraday I* **1980**, *76*, 963.
(9) Pethica, J. B.; Sutton, A. P. *J. Vac. Sci. Technol. A* **1988**, *6*, 2490.
(10) Smith, J. R.; Bozzolo, G.; Banerjea, A.; Ferrante, J. *Phys. Rev. Lett.* **1989**, *63*, 1269.
(11) Attard, P.; Parker, J. L. *Phys. Rev. A* **1992**, *46*, 7959.
(12) Parker, J. L.; Attard, P. *J. Phys. Chem.* **1992**, *96*, 10398.
(13) Greenwood, J. A. *Proc. Roy, Soc. London A* **1997**, *453*, 1277.
(14) Feng, J. Q. *Colloids Surf. A* **2000**, *172*, 175.
(15) Christenson, H. K. *J. Phys. Chem.* **1993**, *97*, 12034.
(16) Campbell, S. D.; Hillier, A. C. *Langmuir* **1999**, *15*, 891.
(17) Schmidtt, F. J.; Ederth, T.; Weidenhammer, P.; Claesson, P.; Jacobasch, H. J. *J. Adhesion Sci. Technol.* **1999**, *13*, 79.
(18) Pashley, M. D.; Pethica, J. B. *J. Vac. Sci. Technol. A* **1985**, *3*, 757.
(19) Horn, R. G.; Israelachvili, J. N.; Pribac, F. *J. Colloid Interface Sci.* **1987**, *115*, 480.
(20) Chen, Y. L.; Helm, C. A.; Israelachvili, J. N. *J. Phys. Chem.* **1991**, *95*, 10736.
(21) Burnham, N. A.; Colton, R. J. *J. Vac. Sci. Technol.* **1989**, *7*, 2906.
(22) Burnham, N. A.; Dominguez, D. D.; Mowery, R. L.; Colton, R. *J. J. Phys. Lett.* **1990**, *64*, 1931.
(23) Weisenhorn, A. L.; Maivald, P.; Butt, H.-J.; Hansma, P. K. *Phys. Rev. B* **1992**, *45*, 11226.
(24) Chaudhury, M. K.; Owen, M. J. *Langmuir* **1993**, *97*, 5722.
(25) Brown, H. R. *Macromolecules* **1993**, *26*, 1666.
(26) Creton, C.; Brown, H. R.; Shull, *K. Macromolecules* **1994**, *27*, 3174.
(27) Deruelle, M.; Leger, L.; Tirrell, M. *Macromolecules* **1995**, *28*, 7419.
(28) Tirrell, M. *Langmuir* **1996**, *12*, 4548.
(29) Attard, P.; Schulz, J.; Rutland, M. W. *Rev. Sci. Instrum.* **1998**, *69*, 3852.
(30) Feiler, A.; Jenkins, P.; Larson, I.; Attard, P. *Langmuir* (in press).
(31) White, L. R. *J. Colloid Interface Sci.* **1983**, *95*, 286.
(32) Landau, L. D.; Lifshitz, E. M. *Theory of Elasticity*, 2nd English ed.; Pergammon: London, 1970.
(33) Attard, P.; Parker, J. L. *J. Phys. Chem.* **1992**, *96*, 5086.
(34) Attard, P.; Mitchell, D. J.; Ninham, B. W. *J. Chem. Phys.* **1988**, *89*, 4358.
(35) Maugis, D.; Barquins M. *J. Phys. D: Appl. Phys.* **1978**, *11*, 1989.
(36) Deruelle, M.; Hervet, H.; Jandeau, G.; Leger, L. *J. Adhes. Sci. Technol.* **1998**, *12*, 225.